Efficient Bidirectional Charge Scheduling for Electric Vehicles: Optimizing Cost and Carbon Emissions

Shizhe Zhao[a,1], Adel N. Toosi[b], Mohammad Goudarzi[c], Muhammad Aamir Cheema[c] and Hao Wang[c]

[a]Shanghai Jiao Tong University, Shanghai, China
[b]University of Melbourne, Melbourne, Australia
[c]Monash University, Melbourne, Australia

ARTICLE INFO

Keywords:
Charge Scheduling
Electric Vehicles
Constrained Optimization
Vehicle-to-Grid

ABSTRACT

Modern Electric Vehicles (EVs) support two-way energy flow, allowing vehicles to both draw power from and supply power to the grid (Vehicle-to-Grid, or V2G). This capability helps reduce carbon emissions and save costs for both EV owners and the grid. The success of V2G systems relies on real-time sensor data from EVs, charging stations, and grid infrastructure, which enables precise monitoring of battery state-of-charge (SoC), grid load, and renewable energy availability. EV owners can charge using renewable energy and discharge surplus energy when renewables are unavailable, taking advantage of lower rates during off-peak hours and selling excess power back during peak demand. Existing works examine the optimal charging and discharging problem from the perspectives of aggregators (charging stations) or operators (grids). This study approaches the problem from the perspective of EV owners, focusing on the scenario where travel plans are well-known in advance. We formulate charging and discharging scheduling as a sequential decision making process and solve it efficiently and optimally using dynamic programming. Experiments show that, in an ideal scenario where green energy are periodically available, an optimal schedule can significantly reduce costs (up to 70%) by selling surplus energy while maintaining a low carbon footprint. ~~where carbon-free green energy are periodically available, an optimal schedule can reduce costs by up to 70% by selling surplus energy while achieving near-zero carbon emissions.~~ In real world scenario where information about price and energy generation are not available, the proposed method also consistently outperforms baselines and aligns better with user preferences.

1. Introduction

The reliance on fossil fuels and the carbon emissions from conventional vehicles contribute significantly to pollution and climate change. In contrast, electric vehicles (EVs) have a low carbon footprint ~~generate nearly zero carbon emissions~~ when charged using renewable energy. Consequently, there is a growing global emphasis on promoting EV research and production, coupled with the establishment of necessary frameworks and environments to make it a viable option for the masses in the near future. Under the Paris Agreement, nearly 193 countries have set a goal for 35% of transport vehicles to be electric by 2035 [1]. Accordingly, there has been a steep rise in the activities of the EV market. The global EV market which was estimated at USD 170 billion in 2021 is expected to reach over USD 1103.17 billion by 2030 [2]. In line with the growing interest in EV, many charging locations have been set across many countries to keep up with the growing demand.

With the advent of bidirectional chargers, EVs can now supply energy to homes, buildings, and the grid, transforming them from mere transportation vehicles into versatile energy storage systems. A recent US survey suggests that automobiles are on the road for nearly 5% of the time, and 90% of the vehicles are unused or parked [3]. Furthermore, typical vehicle owners travel only a short distance every day; for example, the average vehicle owner in Australia drives around 38km daily [4]. This corresponds to less than 10% energy usage for a typical EV battery capacity. When properly incentivized, this surplus energy capacity in EVs can be utilized for sending energy back from the vehicle to the grid (V2G) or vehicle to home (V2H). This can be instrumental in supporting electricity grid

*Corresponding author
shizhe.zhao@sjtu.edu.cn (S. Zhao); adel.toosi@unimelb.edu.au (A.N. Toosi); mohammad.goudarzi@monash.edu (M. Goudarzi); aamir.cheema@monash.edu (M.A. Cheema); hao.wang2@monash.edu (H. Wang)
ORCID(s):
[1]First author

operation, handling energy shortages, blackouts, reducing carbon emissions, and even lowering running costs for EV owners [5, 6].

For EV owners, adopting a strategy of charging vehicles during periods of lower tariffs and discharging to the grid/home during peak tariff times can result in significant monetary gains. Additionally, the reduction of carbon emissions is achievable by charging EVs when excess renewable energy is available and discharging back to the grid/home when renewable energy is less than the energy demand. Charging infrastructures can enhance this potential by incorporating essential discharge points for optimal utilization of V2G benefits. Even parked vehicles at homes, offices, or shopping malls can contribute to this approach by being equipped with charging and discharging points, thereby amplifying the overall advantages of V2G technology.

The challenge for EV owners using V2G technology lies in optimizing their charging and discharging schedules to minimize costs and carbon footprints. With V2G capabilities, EV owners need to strategically charge their vehicles during periods of lower electricity tariffs, ensuring the battery is sufficiently charged for their next journey. At the same time, they should leverage the ability to discharge surplus energy back to the grid or their homes during peak tariff hours, benefiting from higher reimbursement rates. A similar strategy can be adapted to minimize carbon emissions.

In this paper, we investigate the EV charging and discharging scheduling problem from the perspective of EV owners to minimize both the monetary cost of energy consumption and the environmental impact. Considering an EV owner's plan over a specified period, such as a week, we aim to determine a charging/discharging schedule that optimizes an objective function defined as a weighted sum of monetary cost and carbon emissions. For example, given a plan where the owner is at home from 6 pm to 8 am, commutes to work from 8 am to 9 am, and stays at work until 5 pm, the goal is to compute an optimal schedule based on the plan, electricity prices, and other related variables. We incorporate specific EV details like battery capacity and driving efficiency, discretize the time horizon into equal time slots, and perform optimization within these intervals. Considering the charging and discharging prices at each timeslot and the type of energy mix used at each location, we seek to minimize the weighted sum of monetary cost and carbon emissions, with the weight adjustable based on owner preference. The monetary cost also includes battery degradation costs from charging, discharging, and traveling.

We formulate the aforementioned problem as a sequential decision making process, and we assume that full knowledge of factors such as travel plan, carbon intensity and energy price is known in advance. Although there are several works that utilize EVs to minimise the monetary cost or support the grid, these works are orthogonal to our work as we highlight in Section 2. We make several novel contributions in this paper summarized below.

- We formally define the charge/discharge scheduling problem as a sequential decision making process from the perspective of EV owners, aiming to minimize both the monetary cost for owners and carbon emissions. Our model incorporates practical factors, such as realistic charge and discharge electricity prices from the Australian energy context, the carbon footprint of EV operation, and battery degradation.
- We have developed a novel and efficient dynamic programming method to compute the optimal charging and discharging schedule. The proposed approach is lightweight, capable of achieving optimal solutions efficiently, and is both scalable and practical for real-world use cases. It can also serve as a yardstick to evaluate the optimality loss in back-testing for problems that involve partially observable information (see in Sec. 5.4.7).
- We conduct extensive experiments to study the effectiveness of the optimized schedule across diverse scenarios, taking into account for real-world settings and variables such as various EV models, travel plans, and electricity prices. Furthermore, we explore the impact of specific factors, including initial state of charge (SoC), charging and discharging rate, and travel factors, on overall performance. The results demonstrate that, in an ideal scenario where ~~carbon-free~~ green energy are periodically available, the optimized schedule can reduce costs by up to 70% by selling surplus energy while achieving a low carbon emission ~~near zero carbon emissions~~. In real-world scenario, the proposed method also consistently outperforms baselines and aligns better with user preferences.

Limitations. The optimality guarantee of our method depends on certain idealized assumptions, such as perfect knowledge of prices, carbon intensity, and travel plans. These assumptions may result in optimality loss or limitations in real-world applications, causing the experiment results to not be representative in broader scenarios. Readers can find more details about optimality loss in Section 5.4.7 and a discussion on limitations in Section 6.

The rest of the paper is organized as follows. Section 2 reviews related work and highlights the differences from our approach. In Section 3, we formally define the problem. Our dynamic programming method is detailed in Section 4. Section 5 presents an extensive experimental study. Finally, conclusions and future work are discussed in Section 6.

2. Related Works

Existing works related to charging and discharging scheduling can be classified into two categories: user-centric and system-centric.

User-centric works focus on decisions that related to a EV trip, and usually assume full knowledges about the trip are known in advance. Blatiak et al. [7] studies day-ahead scheduling aiming at balancing electricity service and solve a mixed integer programming to determine decisions on trip starting times. Liu et al. [8] integrate route selection and charging/discharging control to minimize operational cost while satisfy trip-related constraints. The problem is addressed in a two stage framework: initially finding K candidate trips-related decisions, then applying mixed integer programming to assign these decisions to EVs. Likewise, other researchers conducts charging station matching for EVs to reduce operational cost [9], minimize surplus energy [10], or improve service quality [11]. Du et al. [12] focus on designing techniques for individual taxi drivers or delivery service providers leveraging bidirectional charging to optimise the profit. In addition, a line of work delves deeply into the battery degradation model to better estimate charging and discharging outcomes [13, 14].

In this work, under the assumption of full knowledge, we examine the problem involving a sequence of trips for a single EV, where decisions for each trip are interconnected due to constraints and objectives (see in Sec. 3).

System-centric works study the problem from the perspectives of aggregators (e.g., charging stations) or operator (e.g., grids), where involving partial observable information. Daina et al. [15] develop a random utility model to capture users' behavior in traveling and charging, which can support decision making in an energy system. Krueger et al. [16] actively capture user preference on-the-fly and the controller in charging station can generate charging/discharging instructions accordingly. In [17], the authors propose an award-penalty mechanism to mitigate the impact of users' unexpected behavior. Zhao et al. [18] combines an online booking system with a pricing-based charging control system to shift demand from peak to off-peak times. Aljafari et al. [19] explore optimizing EV charging station management to minimize waiting times and reduce electricity costs for EV users. Similarly, Saldarini et al. [20] reveals the crucial role of real-time communication in reducing charging waiting time. In addition, Koufakis et al. [21] employs an online-offline framework that solves the problem offline with the full knowledge assumption, and integrate it with an online algorithm to handle new information in real-time. Another line of work studies the problem from the perspective of grid operator [22–25], which consider multi-objectives explicitly aimed at optimization from an energy system point of view.

In this work, we focus on user-centric problem that does not involve partial observable information, prices strategy and energy generation decisions.

3. Problem Formulation

3.1. Input

The time horizon $\mathbb{T}$ is divided into t disjoint, contiguous and equal-sized timeslots, i.e., $\mathbb{T} = \{\mathcal{T}_1, \cdots, \mathcal{T}_t\}$. The length of each timeslot $\mathcal{T}_i \in \mathbb{T}$ is Δt time units. We are given a plan $\mathbb{L}$ of the EV owner for the time horizon $\mathbb{T}$ where each $\mathcal{L}_i \in \mathbb{L}$ denotes the location of the EV at timeslot $\mathcal{T}_i$. Note that, if $\mathcal{L}_i \neq \mathcal{L}_{i+1}$, this implies that the EV owner will be driving during timeslot $\mathcal{T}_i$. For each location $\mathcal{L}_i$, we are also giving the following:

- $\mathcal{P}_i^{ch}$: The charging rate in kW at which energy can be transmitted from the charger to the EV at location $\mathcal{L}_i$ at timeslot $\mathcal{T}_i$. If $\mathcal{L}_i$ is a location which does not have charging facility at $\mathcal{T}_i$, $\mathcal{P}_i^{ch}$ is set to zero.
- $\mathcal{P}_i^{dis}$: The discharging rate in kW at which energy can be transmitted from the EV to the charging location $\mathcal{L}_i$ at timeslot $\mathcal{T}_i$. If $\mathcal{L}_i$ is a location which does not have discharging facility at $\mathcal{T}_i$, $\mathcal{P}_i^{dis}$ is set to zero.
- P_i^B: The buying (charging) price at $\mathcal{L}_i$ at $\mathcal{T}_i$ in \$ per kWh.
- P_i^S: The selling (discharging) price at $\mathcal{L}_i$ at $\mathcal{T}_i$ in \$ per kWh.
- E_i: The emission intensity (in grams of CO2 per kWh) at $\mathcal{L}_i$ at $\mathcal{T}_i$. This depends on the source of energy, e.g., solar, fossil fuel, a mix etc.
- α: A user-chosen value representing the user's preference between reducing CO2 emissions and saving costs (see details in 3.2).

Symbol	Meaning
$\mathbb{T}$	The set of discretized timeslots
$\mathcal{T}_i$	$\mathcal{T}_i \in \mathbb{T}$ a timeslot with duration of Δt time units
$\mathbb{L}$	Plan for $\mathbb{T}$
$\mathcal{L}_i$	$\mathcal{L}_i \in \mathbb{L}$, The location of EV at timeslot $\mathcal{T}_i$
$\mathcal{P}_i^{ch}$	The energy rate for charging EV at $\mathcal{L}_i$ at $\mathcal{T}_i$
$\mathcal{P}_i^{dis}$	The energy rate for discharging EV at $\mathcal{L}_i$ at $\mathcal{T}_i$
P_i^B	The buying (charging) price at $\mathcal{L}_i$ at $\mathcal{T}_i$ in \$ per kWh.
P_i^S	The selling (discharging) price at $\mathcal{L}_i$ at $\mathcal{T}_i$ in \$ per kWh
E_i	The emission intensity in grams of CO2 per kWh at $\mathcal{L}_i$ at $\mathcal{T}_i$.
B_{cst}	The EV battery cost in dollars
B_c	The EV battery capacity in kWh
D^E	The EV driving efficiency in kWh per km
SoC_i	The SoC of the EV battery at the end of timeslot $\mathcal{T}_i$
d_i	The distance travelled by the EV during the timeslot $\mathcal{T}_i$
$\mathbb{C}^{\$}$	The total monetary cost of the EV owner over $\mathbb{T}$
$\mathbb{C}^{CO2}$	The total emission cost of the EV owner over $\mathbb{T}$
α	The preference weight for the monetary cost, $0 \leq \alpha \leq 1$
$1-\alpha$	The preference weight for emission cost, $0 \leq \alpha \leq 1$
$C_i^{\$}$	The monetary cost at timeslot $\mathcal{T}_i$
C_i^{CO2}	The emission cost at timeslot $\mathcal{T}_i$
C_i^B	The cost for buying electricity at $\mathcal{T}_i$
C_i^S	The cost for selling electricity at $\mathcal{T}_i$
C_i^{DEG}	The battery degradation cost at $\mathcal{T}_i$
X_i^B	The binary decision variable if EV is charged (buying) at $\mathcal{T}_i$
X_i^S	The binary decision variable if EV is discharged (selling) at $\mathcal{T}_i$
SoC^{max}	The maximum possible charge level across timeslots
SoC^{min}	The minimum possible charge level across timeslots
μ	The battery cycle efficiency

Table 1
Table of Notations

We assume that the EV is plugged-in at $\mathcal{L}_i$ for every $\mathcal{T}_i$ as long as it is not travelling during $\mathcal{T}_i$. In other words, the EV can be charged or discharged at these locations if needed. . Additionally, the input includes the following information specific to the EV. The EV battery cost in dollars (B_{cst}), EV battery capacity in kWh (B_c), EV driving efficiency in kWh per km (D^E). Let SoC_i be the state of charge (SoC) of the EV battery at the end of timeslot $\mathcal{T}_i$. The SoC of the EV battery at the beginning of the first timeslot, i.e., SoC_0, is given. We define $\Delta SoC_i = SoC_i - SoC_{i-1}$ as the amount of charge the battery receives during timeslot $\mathcal{T}_i$ (which can be a negative value if the battery was discharged). If the EV is driving at timeslot $\mathcal{T}_i$ (i.e., $\mathcal{L}_i \neq \mathcal{L}_{i+1}$), ΔSoC_i is calculated as follows:

$$\Delta SoC_i = -\frac{D^E \times d_i}{B_c}, \quad \text{if } \mathcal{L}_i \neq \mathcal{L}_{i+1}, \tag{1}$$

where D^E is the driving efficiency (energy used per km of driving), d_i is the distance travelled during the timeslot $\mathcal{T}_i$ and B_c is the battery capacity. Note that ΔSoC_i is negative indicating that the battery is discharged during timeslot $\mathcal{T}_i$. We remark that more accurate estimation of energy consumed for the travel can be easily calculated if required by using the actual route from $\mathcal{L}_i$ to $\mathcal{L}_{i+1}$ and using energy estimation models that consider the factors such as route, speed, acceleration and idle time to better estimate the energy consumption. Here, for the sake of simplicity, we use the length of the route d_i and the driving efficiency D^E to estimate the energy consumption.

If the vehicle is charging (i.e., buying electricity), ΔSoC_i is computed as follows:

$$\Delta SoC_i = \frac{\mathcal{P}_i^{ch} \times \Delta t}{B_c}, \quad \text{if } \textit{charging} \tag{2}$$

where $\mathcal{P}_i^{ch}$ is the charging power at location $\mathcal{L}_i$ at timeslot $\mathcal{T}_i$ and Δt is the length of each timeslot. When the vehicle is selling electricity, ΔSoC_i is computed similarly but is negative.

$$\Delta SoC_i = -\frac{\mathcal{P}_i^{dis} \times \Delta t}{B_c}, \quad \text{if } discharging \tag{3}$$

3.2. Optimisation Problem

The objective is to minimize the total cost, which is defined as the weighted sum of two components: (1) the *monetary* cost, denoted as $\mathbb{C}^{\$}$, which includes the expenses associated with buying and selling electricity as well as the battery degradation due to charging, discharging, and driving; and (2) the *emission* cost, denoted as $\mathbb{C}^{CO2}$. Formally, the goal is to minimize the objective function given by the following expression:

$$\min \mathbb{C}_T,$$

where

$$\mathbb{C}_T = \alpha \times \mathbb{C}^{\$} + (1-\alpha) \times \mathbb{C}^{CO2},$$

where α is the weight in the weighted sum and $0 \leq \alpha \leq 1$. We employ min-max normalisation on both $\mathbb{C}^{\$}$ and $\mathbb{C}^{CO2}$ before applying the weighted sum to ensure they share a consistent scale. Next, we formalise how $\mathbb{C}^{\$}$ and $\mathbb{C}^{CO2}$ are computed.

$\mathbb{C}^{\$}$ is the total monetary cost incurred during all timeslots computed as follows

$$\mathbb{C}^{\$} = \sum_{\mathcal{T}_i \in \mathcal{T}} C_i^{\$}, \tag{4}$$

where $C_i^{\$}$ is the cost at timeslot $\mathcal{T}_i$ computed as

$$C_i^{\$} = C_i^B + C_i^S + C_i^{DEG}. \tag{5}$$

Here, C_i^B is the cost for buying electricity at $\mathcal{T}_i$ (Eq. (6)), C_i^S is the cost for selling electricity at $\mathcal{T}_i$ (Eq. (7)) and C_i^{DEG} is the battery degradation cost at $\mathcal{T}_i$ (Eq. (8)).

$$C_i^B = X_i^B \times \Delta SoC_i \times B_c \times P_i^B, \tag{6}$$

where X_i^B is a decision variable which is 1 if the EV buys electricity (i.e., is charged) at timeslot $\mathcal{T}_i$, otherwise 0. Here, $\Delta SoC_i = SoC_i - SoC_{i-1}$ is the difference in the state of charge during the timeslot $\mathcal{T}_i$, e.g., if the battery was 40% charged at the beginning of $\mathcal{T}_i$ and was 50% charged at the end, ΔSoC_i is 0.1 (or 10%). Recall that B_c is the battery capacity in kWh and multiplying B_c with ΔSoC_i gives the amount of energy in kWh bought at timeslot $\mathcal{T}_i$. Finally, P_i^B is the buying price of electricity (in dollars per kWh) at the location L_i at timeslot $\mathcal{T}_i$.

Similarly,

$$C_i^S = X_i^S \times \Delta SoC_i \times B_c \times P_i^S, \tag{7}$$

where X_i^S is a decision variable which is 1 if the EV sold the electricity back to grid/home at timeslot $\mathcal{T}_i$, otherwise 0. Note that, at any timeslot $\mathcal{T}_i$, only one of X_i^B or X_i^S can be 1 (i.e., a vehicle cannot buy and sell during the same timeslot). Furthermore, when the vehicle is travelling during timeslot $\mathcal{T}_i$ (i.e., $\mathcal{L}_i \neq \mathcal{L}_{i+1}$), both X_i^B and X_i^S are 0, i.e., buying/selling is not allowed in a timeslot when the vehicle is travelling. P_i^S is the selling price at location $\mathcal{L}_i$ at timeslot $\mathcal{T}_i$. Note that, if the vehicle sells the electricity, ΔSoC_i is negative (see Eq. (3)), thus, the cost C_i^S is negative, implying that the EV owner earned money during the timeslot.

$$C_i^{DEG} = \frac{B_{cst}}{2 \times \mu^2 \times a} \times |(1 - SoC_{i-1})^b - (1 - SoC_i)^b|. \tag{8}$$

C_i^{DEG} is the battery degradation cost incurred during timeslot $\mathcal{T}_i$ which depends on SoC at the beginning and end of the timeslot, total battery cost B_{cst}, the battery cycle efficiency μ and two battery specific variables a and b (see [26]). Note that the degradation cost is zero when there is no buying, selling or traveling during the timeslot (i.e., SoC remains unchanged). Our proposed solution can use any battery degradation model. However, the degradation cost can be approximated to a linear function if required for the optimisation solver.

$\mathbb{C}^{CO2}$ is the summation of CO_2 emission costs over all timeslots.

$$\mathbb{C}^{CO2} = \sum_{\mathcal{T}_i \in \mathcal{T}} C_i^{CO2}, \tag{9}$$

where C_i^{CO2} is the emission cost at timeslot $\mathcal{T}_i$. We make the assumption that the emission cost is accrued during the purchase of electricity and is calculated as follows

$$C_i^{CO2} = X_i^B \times \Delta SoC_i \times B_c \times E_i, \tag{10}$$

where X_i^B is the decision variable introduced above which is 1 if the EV was charged at timeslot $\mathcal{T}_i$, otherwise 0. $\Delta SoC_i \times B_c$ gives the amount of energy (in kWh) bought during $\mathcal{T}_i$ and E_i is the emission intensity (in grams of CO2 per kWh) of the charging at $\mathcal{L}_i$ at $\mathcal{T}_i$.

3.3. Constraints

In this section, we define the constraints for the optimisation problem. A user may not want to charge above a certain level SoC^{max} or discharge below a certain level SoC^{min}. This constraint is defined for each timeslot $\mathcal{T}_i \in \mathcal{T}$ as follows.

$$0 \leq SoC^{min} \leq SoC_i \leq SoC^{max} \leq 1. \tag{11}$$

Additionally, we introduce another constraint that the SoC at the end of the time horizon must be at least equal to a user-defined value τ.

$$SoC_t \geq \tau, \tag{12}$$

This constraint is necessary to ensure that the battery's SoC is maintained at or above the specified τ value at the end of the schedule. Without this constraint, the SoC could potentially drop to SoC^{min} which may not be desirable by the EV owner.

The optimisation needs to determine the binary decision variables X_i^B and X_i^S at each timeslot $\mathcal{T}_i$. At any timeslot at most one of X_i^B and X_i^S can be 1. These constraints are defined as follows.

$$X_i^S \in \{0, 1\}, \tag{13}$$
$$X_i^B \in \{0, 1\}, \tag{14}$$
$$X_i^B + X_i^S \leq 1. \tag{15}$$

X_i^B and X_i^S variables must be zero at a timeslot $\mathcal{T}_i$ during which the vehicle is driving.

$$X_i^B = 0, \quad if\, \mathcal{L}_i \neq \mathcal{L}_{i+1}, \tag{16}$$
$$X_i^S = 0, \quad if\, \mathcal{L}_i \neq \mathcal{L}_{i+1}. \tag{17}$$

The optimization problem discussed in this section is a mixed-integer problem, commonly tackled using tools like MiniZinc[2] and solvers such as Gurobi,[3] as we attempted in our approach. However, solvers exhibit limited scalability when addressing large-scale problems, frequently failing to generate results for numerous instances in our experiments. This limitation is primarily attributed to their high computational complexity, which constrains their effectiveness in handling extensive datasets and complex problem domains. Consequently, we aim to achieve optimal results more efficiently by employing dynamic programming techniques.

[2] https://www.minizinc.org/
[3] https://www.gurobi.com/

4. Our Proposed Solution

We propose an efficient dynamic programming (DP) algorithm to find the optimal solution to the problem discussed in the previous section. We discretize SoC into $\mathcal{S}$ discrete values. Our proposed DP algorithm runs in $O(|\mathbb{T}|\times\mathcal{S})$ where $|\mathbb{T}|$ is the total number of timeslots and $\mathcal{S}$ is the number of discrete SoC values used by the DP algorithm.

We create a two dimensional array *opt* to memorize the optimal results of the subproblems. Specifically, $opt[i][s]$ stores the minimum cost for any schedule until (and including) the timeslot $\mathcal{T}_i$ such that the SoC of the EV following the schedule is s at the end of $\mathcal{T}_i$, i.e., $SoC_i = s$.

The array *opt* consists of $|\mathbb{T}|+1$ rows, representing timeslots from 0 to $|\mathbb{T}|$, and $\mathcal{S}$ columns, representing discretized SoC values. All values in the array are initially set to infinity, with the exception of $opt[0][SoC_0]$, which is set to zero. This initialization indicates that the minimum cost at the beginning of the plan is zero.

There are four possible actions for the EV at a timeslot $\mathcal{T}_i$: i) EV owner is driving (D); ii) EV is buying electricity (B); ii) EV is selling electricity (S); iv) none of the above (N). We use ΔSoC_i^D, ΔSoC_i^B, ΔSoC_i^S and ΔSoC_i^N to denote the change in SoC during the timeslot $\mathcal{T}_i$ for each of these possible actions, respectively. Note that $\Delta SoC_i^N = 0$ whereas ΔSoC_i^D, ΔSoC_i^B and ΔSoC_i^S are computed using Equations (1), (2) and (3), respectively. Let A denote the set of possible actions, i.e., $a \in A = \{D, B, S, N\}$, we formalise ΔSoC_i for each of these actions as follows:

$$\Delta SoC_i^a = \begin{cases} -\dfrac{D^E \times d_i}{B_c} & \text{if } a = D \\ \dfrac{\mathcal{P}_i^{ch} \times \Delta t}{B_c} & \text{if } a = B \\ -\dfrac{\mathcal{P}_i^{dis} \times \Delta t}{B_c} & \text{if } a = S \\ 0 & \text{if } a = N \end{cases} \tag{18}$$

Let $\mathbb{C}_i^a$ be the total cost incurred during timeslot $\mathcal{T}_i$ if the action during this timeslot is $a \in \{D, B, S, N\}$. Here, $\mathbb{C}_i^a = \alpha \times C_i^{\$} + (1-\alpha) \times C_i^{CO2}$ where $C_i^{\$}$ is the monetary cost of driving/buying/selling during $\mathcal{T}_i$ (see Eq. (5)) and C_i^{CO2} is the emission incurred during $\mathcal{T}_i$ (see Eq. (10)). For the calculation of these, the decision variable X_i^B is set to 1 only if the EV is buying electricity ($a = B$), X_i^S is set to 1 only if the EV is selling electricity ($a = S$), otherwise (i.e., $a = D$ or $a = N$) both are set to 0. Note that this translates to $\mathbb{C}_i^N = 0$ and $\mathbb{C}_i^D$ to be equal to the battery degradation cost due to the driving.

Now, we describe the optimal substructure of the problem by showing how to compute $opt[i][s]$ by using the optimal values of the subproblems computed and stored in the *opt* array earlier. To satisfy the constraints in Eq. (11), we consider $opt[i][s]$ to be infinity for any s for which either $s < SoC^{min}$ or $s > SoC^{max}$. Note that if the EV owner is driving during $\mathcal{T}_i$ (i.e., $\mathcal{L}_i \neq \mathcal{L}_{i+1}$) then the other actions such as buying and selling electricity are not possible. Otherwise, we compute the optimal value by considering each possible action and choose the minimum. This is formalised as shown below.

$$opt[i][s] = \begin{cases} \infty, & \text{if } s < SoC^{min} \text{ or } s > SoC^{max} \\ \mathbb{C}_i^D + opt[i-1][s - \Delta SoC_i^D], & \text{if } \mathcal{L}_i \neq \mathcal{L}_{i+1} \\ \min\limits_{a \in \{B,S,N\}} \mathbb{C}_i^a + opt[i-1][s - \Delta SoC_i^a], & \text{otherwise} \end{cases} \tag{19}$$

The array *opt* is filled in a bottom-up approach, i.e., we compute $opt[i][s]$ for each i in increasing order, where for each row i, we compute $opt[i][s]$ in increasing order of s. At the end, we go through the last row $opt[|\mathbb{T}|]$ and the optimal value is the smallest value $opt[|\mathbb{T}|][s]$ that satisfies the constraint in Eq. (12), i.e., $s \geq \tau$. Formally, the optimal solution $\min \mathbb{C}_T$ to the problem is

$$\min \mathbb{C}_T = \min_{\forall s \geq \tau} opt[|\mathbb{T}|][s] \tag{20}$$

Algorithm 1: Dynamic programming

Input: SoC_1: initial sum of charge;
t: max time slot;

$opt[*][*] \leftarrow \infty$;
$opt[0][SoC_0] \leftarrow 0$;
for $i = 1 \cdots t$ **do**
  for $s = SoC^{min} \cdots SoC^{max}$ **do**
    if $\mathcal{L}_i = \mathcal{L}_{i+1}$ **then**
      for $a \in \{B, S, N\}$ **do**
        $\Delta SoC_i^a \leftarrow$ Eq. (18);
        $opt[i][s] \leftarrow \min(opt[i][s], opt[i-1][s - \Delta SoC_i^a])$
    else
      $\Delta SoC_i^D \leftarrow$ Eq. (18);
      $opt[i][s] \leftarrow \mathbb{C}_i^D + opt[i-1][s - \Delta SoC_i^D]$;
return $\min_{\forall s \geq \tau} opt[|\mathbb{T}|][s]$

For each $opt[i][s]$, in addition to the optimal value, we also maintain the optimal action $a \in \{D, B, S, N\}$ leading to the optimal value. This can be used to construct the optimal action plan that results in the minimum cost $\min \mathbb{C}_T$. Algorithm 1 demonstrate the pseudo code.

4.1. Discussion

Impact of discretization Discretizing the SoC introduces rounding error that is accumulated over the time horizon, known as accumulated rounding error (ARE). For example, when the max rounding error per transition is 0.01% (i.e., with two decimal points of discretization), for a horizon of 336 timeslots (e.g., one week with 30 min per timeslot), the worst-case ARE on SoC can be up to 3.36%. ARE causes two problems:

- DP may generate an infeasible plan that reaches a $SoC_i < SoC^{min}$ state during execution. In practice, this can be avoided by applying a safety margin in the planning. Specifically, at the timeslot t, we ensure $SoC_i \geq SoC^{min} + 0.01\%t$.
- DP may miss an optimal solution if ARE is too large. When optimality is critical, we can increase the number of decimal points until the schedule remains unchanged.

Scalability and granularity Since the number of state of DP is $O(|\mathbb{T}| \times S)$, one might expect its runtime increases linearly with the number timeslots. However, due to ARE, increasing the number of timeslots also requires increasing the granularity (i.e., S) to maintain the same level of ARE. This means that when preserving ARE is critical, the runtime increases quadratically with the number of timeslots.

Pareto frontiers Pareto frontiers contains all possible plans that are not dominated. When dealing with multiple objectives, there is always a trade-off between combining them into a single function or finding all Pareto frontiers. The latter may result into a lot of plans being returned to the users, which can be overwhelming. In Sec. 6 we discuss potential directions about Pareto frontiers in future work.

Grid constraints In this work, we study the problem from users perspective. Therefore, many constraints, such as aggregator coordination and grid limits, are not considered. However, in practice, some grid constraints can be communicated in real times and adapted to DP. For example, $\mathcal{P}_i^{ch}$ and $\mathcal{P}_i^{dis}$ can be set to zero to imitate the scenarios where the location with charging and discharging facility disabled by grid. We can then re-plan in DP to reflect the real-time updates.

5. Performance Evaluation

In this section, we evaluate the performance of different approaches in synthetic dataset and real-world dataset. In synthetic dataset, we focus on the two common user profiles and examine how various factors impact the schedule. In real-world dataset, we assess the performance of the proposed method with various level of granularity and carbon intensity.

5.1. Baseline Approaches

We benchmark our proposed method against several baseline approaches. We use V1G to refer to the smart charging approaches that decide when to charge but are not allowed to sell/discharge electricity. We use V2G to refer to the approaches allowed to sell electricity and decide when to charge or discharge. Additionally, we consider some simple charging approaches that assume that the user always plugs-in their EV at certain locations/times to charge the EV. Below are the details of the approaches:

- *Opt-V2G*: This is our proposed DP solution in Section 4 that returns the optimal solution for the problem defined in Section 3.
- *Opt-V1G*: This baseline approach returns the optimal solution when selling electricity is not allowed. Specifically, it produces an optimal solution to the problem defined in Section 3, assuming that the selling decision is never made, i.e., X_i^s is zero for every timeslot $\mathcal{T}_i$. We modify our DP algorithm to obtain the optimal solution by ensuring that selling is impossible at every timeslot, i.e., $S \notin A$.
- *Greedy-V2G*: This is a greedy solution to the problem defined in Section 3. This approach makes selling decisions greedily, as long as it reduces the objective

$$\alpha \times C_i^{\$} + (1-\alpha) \times C_i^{CO2} \tag{21}$$

  under the given α at the current time slot i. It also ensures that the EV has enough SoC for the next trip it needs to take, and other constraints on the SoC are satisfied (see Eq. (11) and Eq. (12)). Since this approach only considers that the EV has enough SoC for the next trip, in some cases, it may not guarantee finding a feasible schedule, e.g., after performing the next trip, the EV may not have enough SoC and may not have enough time to charge for the subsequent trips.
- *Greedy-V1G*: This approach is the same as Greedy-V2G except that it does not make discharging (selling) decisions.
- *Plug-in approaches*: Three typical charging approaches are considered: @Home, ¬Home, and @Solar. These approaches focus solely on charging, assuming that the user consistently plugs in their EV at designated locations or during specific times. Whenever the EV is plugged-in, the EV is assumed to be charging unless the SoC reaches SoC^{max}.
  - @*Home*: The user always plugs-in their EV to the charger whenever they are at home.
  - ¬*Home*: The user always plugs-in their EV at every location other than home, e.g., an apartment dweller without access to a home charger.
  - @*Solar*: The user always plugs-in their EV whenever solar energy is available.

  While other typical charging behaviors exist, these three represent common charging patterns and the goal is to assess how other approaches perform relative to these typical user behaviors. Note that Opt-V1G is the optimal charging strategy and always outperforms these charging behaviors in terms of the objective function defined in Section 3.

All the approaches mentioned above are deterministic, meaning that for the same input, the output is always the same. Therefore, all instances are evaluated only once, and data entries regarding CO2 and cost should have no variability unless explicitly mentioned. We discretise ΔSoC_i with precision two decimal points (e.g., 50.85%) to ensure the accumulated errors (ARE) are not significant, i.e., $S = 10,000$ and the worst-case ARE on SoC is 3.36%. It is worth

Table 2
Plans for different EV user types. ⚡ shows that the EV is plugged into a charger, and 🚗 shows driving.

	EV User Types	Category	Plans			
Sedentary	Office-Morning	Weekdays	🚗 08:00-09:00 (40 km)	⚡Office 09:00-17:00	🚗 17:00-18:00 (40 km)	⚡Home 18:00-08:00
	Office-Afternoon	Weekdays	🚗 14:00-15:00 (40 km)	⚡Office 15:00-23:00	🚗 23:00-00:00 (40 km)	⚡Home 00:00-14:00
	Office-Night	Weekdays	🚗 23:00-00:00 (40 km)	⚡Office 00:00-08:00	🚗 08:00-09:00 (40 km)	⚡Home 09:00-23:00
	All	Weekend	🚗 10:00-11:00 (30 km)	⚡Shopping 11:00-12:00	🚗 12:00-13:00 (30 km)	⚡Home 13:00-10:00
Mobile	Taxi-Morning	Weekdays	🚗 09:00-12:00 (99 km)	⚡Shopping 12:00-13:00	🚗 13:00-17:00 (131 km)	⚡Home 17:00-09:00
	Taxi-Afternoon	Weekdays	🚗 15:00-18:00 (99 km)	⚡Shopping 18:00-19:00	🚗 19:00-23:00 (131 km)	⚡Home 23:00-15:00
	Taxi-Night	Weekdays	🚗 00:00-03:00 (99 km)	⚡Shopping 03:00-04:00	🚗 04:00-08:00 (131 km)	⚡Home 08:00-00:00
	All	Weekend	🚗 10:00-11:00 (30 km)	⚡Shopping 11:00-12:00	🚗 12:00-13:00 (30 km)	⚡Home 13:00-10:00

Table 3
Energy prices [27] and carbon intensity [28] for various locations.

Location and time	Charging price ($/kWh)	Discharging price ($/kWh)	Emission (g/kWh)
Home-offpeak (00:00-07:00 and 21:00-00:00)	0.27	0.27	820
Home-onpeak (19:00-21:00)	0.47	0.47	820
Home-solar (07:00-19:00)	0.05	0.05	0
Office-Complementary (24 hrs)	0	0	410
Office-Paid (24 hrs)	0.15	0.15	410
Shopping Center (24 hrs)	0.30	0.15	410

mentioning that AREs are usually very small. For example, in all experiments, we found that AREs are less than 0.01%. All approaches are implemented in Python and experiments are run on a computer with *Intel Xeon E-2276M* processor and *32 GB* RAM. EV states are represented in a discrete space in our optimisation model. The length of each timeslot is 30 min.

5.2. Test scenarios

We evaluate the performance of approaches for different types of EV users. Since this work focus on scenarios where the travel patterns of users are well-known in advance, two typical user profiles are considered: office workers who commute regularly on weekdays, and taxi drivers who usually know the duration of their shifts in advance.

5.2.1. Plans

To create plans, we consider two key groups of EV users: sedentary users (such as office workers, retail employees, hospital staff, and factory workers) and mobile users (including taxi drivers, delivery personnel, and Uber drivers). For simplicity, we designate these user types as "office worker" and "taxi driver". For each type of EV user, we consider three distinct shift timings corresponding to their work start times: i) morning (9:00 to 17:00); ii) afternoon (15:00 to 23:00); and iii) night (00:00 to 08:00). This results in a total of six unique plans, with each EV user type having three different working hour combinations. Each plan is denoted as `userType-workingHours`, e.g., Taxi-Night denotes a taxi driver who works during the night and Office-Afternoon denotes an office worker whose shift starts in the afternoon.

Next, we describe the charging and travel routine of the office worker and the taxi driver as shown in Table 2. We assume that each EV user works 5 days a week (called weekdays) and takes 2 days off (called weekend). A weekly schedule consists of 336 time slots each of 30 mins duration, and the first and last day of a week are always weekend.

Office Worker During the weekdays, the office worker's routine involves driving to the office to reach at the start of their shift, leaving the EV parked at the office throughout the working hours, and finally returning home after work. Outside of the working hours, they remain at home. During the weekend, the EV owner stays at home the whole day except between 10:00 am to 01:00 pm (Fig. 1(a)). Specifically, the EV owner departs home at 10:00 am to visit a shopping center, stays at the shopping center for 1-hour, and then returns back home. We assume that the office and the shopping center are 40 km and 30 km from home, respectively. Later, we vary the daily traveling distance/time to study its effect. Since we discretize each timeslot to 0.5 hour, we assume each action takes at least 0.5 hour (e.g., driving to a shopping center takes 1 hour).

Taxi Driver During the weekdays, the taxi driver initiates their workday by leaving home at the start of their working hours and concluding it by returning home after completing their shift. Our model assumes a one-hour break for the taxi driver halfway through their shift, during which they park at a shopping center with charging/discharging capabilities.

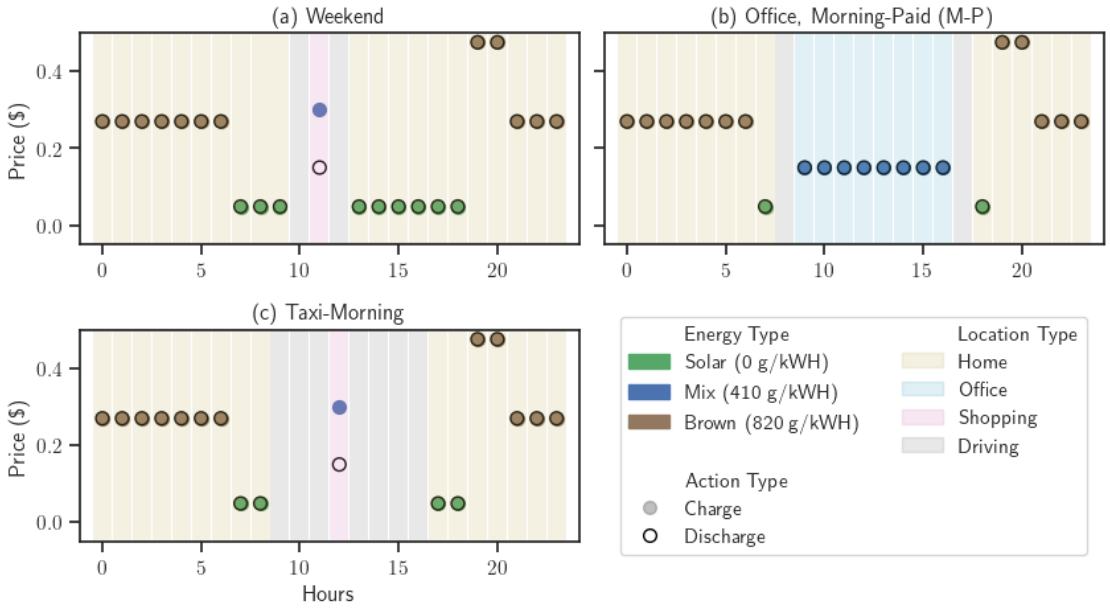

Figure 1: The travel routines of an office worker and a taxi driver are shown both on a weekend and a weekday morning shift. Each plot consists of 24 vertical bars, with each bar representing an hour of the day. The color of a bar indicates the user's location during that time. Solid and hollow circles at each bar represent the price on charging and discharging, respectively. The color of the solid circle indicates the energy type when charging. The prices for changing and discharging do not necessary have to be the same.

The taxi driver covers a daily distance of 230 km during an 8-hour shift, incorporating 7 hours of driving and a 1-hour break. This distance is evenly distributed across each working hour, equating to an average speed of approximately 32.8 km per hour.[4] The weekend routine of the taxi driver is the same as the office worker.

5.2.2. Energy prices and carbon intensity

There are three types of energy sources: *solar*, *mix*, and *brown*, with carbon intensities E_i of 0 g/kWH, 410 g/kWh, and 820 g/kWh [28]. Next, we describe details of the energy prices and carbon intensity for each location of the EV throughout the week, as shown in Table 3. All costs reported in the paper are in Australian dollar (AUD).

Home We assume the home is equipped with rooftop solar panels and utilises the actual tariffs applicable in Victoria, Australia. When the vehicle is parked at home, the electricity pricing adheres to the solar tariff during the daytime (07:00 - 19:00) and the standard two-period time-of-use tariff at other times. We set the electricity prices of buying and selling for the EV at home to be the same. This means that if an EV supplies power to the home, it effectively offsets the costs that the EV owner would otherwise have to pay to the grid. During daylight hours (07:00 to 19:00), the solar tariff is in effect, offering electricity at a rate of 0.05 $/kW with an emission intensity of 0 g/kWh. It is important to note that solar energy is not considered free because any surplus not used to charge the EV is sold back to the grid at a feed-in-tariff rate of 0.05 $/kWh. At all other times, only brown energy is available with an emission intensity of 820 g/kWh. The off-peak rate (00:00 to 07:00 and 21:00 to 00:00) is set at 0.27 $/kWh, while the on-peak rate (19:00 to 21:00) is 0.47 $/kWh.

Office When the Office Worker parks at office during the working hours on weekdays, we consider two types of scenarios: i) the office offers complementary charging to the EV owners to encourage EV adoption; ii) the office offers charging at 0.15 $/kWh. The charging and discharging prices at the office are assumed to be the same. The energy source at the office is considered to be a mix of brown and green energy with an emission intensity of 410 g/kWh.

[4] https://www.atia.com.au/wp-content/uploads/2014-State-Territory-Taxi-Statistics.pdf

Table 4
Default Values

Parameter	Default value
α	0.5
SoC_0	70%
τ	SoC_0
SoC^{min}	20%
SoC^{max}	80%
μ	0.95 [26]
$\mathcal{P}_i^{ch}$	7.2 kW [30]
$\mathcal{P}_i^{dis}$	7.2 kW [30]
Scenario	Officer worker, Morning Shift
Vehicle Model	BYD Atto ($D^E = 183, B_c = 60$) [29]
Office Energy supplies	Complementary

Shopping Center When the EV is at the shopping center (during the weekend for both types of EV users or during the shift break for the taxi driver), the electricity prices of buying and selling are set to 0.30 \$/kWh and 0.15 \$/kWh, respectively. The energy source is assumed to be mixed with an emission intensity of 410 g/kWh.

Fig. 1 shows an example of travel routines for an office worker and a taxi driver, both on a weekend and on a weekday morning shift.

5.2.3. Other settings

The user's EV, a BYD Atto 3, features a battery capacity (B_c) of 60 kWh and a driving efficiency (D^E) of 183 Wh/km [29]. Note that the battery cost (B_{cst}) is required to calculate the battery degradation cost, as outlined in Eq. (8). We calculate the battery cost by multiplying battery capacity B_c with \$229 which is the cost[5] of EV battery per kWh. To illustrate, the cost of BYD Atto 3 battery (60 kWh) is $229 \times 60 = 13,740$ dollars. As a default setting, we assume that the charger at each location (i.e., home, office, and shopping center) is a level-2 charger with a charging/discharging rate of 7.2kW [30]. Also, we study the effect of other types of EVs with different battery capacity and driving efficiency. We set SoC^{min} and SoC^{max} to 0.2 and 0.8, respectively (see Eq. (11)). The default SoC at the start of the schedule, SoC_0, is 0.7. We require that the SoC at the end of the schedule be at least equal to the initial SoC, i.e., $\tau = SoC_0$ in Eq. (12). The default value of α is also set to 0.5. To study the impact of SoC_0 and α, we vary these values in different experiments. Table 4 shows a summary of default values.

5.3. Results for different test scenarios

5.3.1. Office Worker

Fig. 2 shows the results for different test scenarios for the Office Worker described in the previous section. Each scenario is denoted as two letters separated by a hyphen (e.g., M-C) where the first one denotes the working hours (M, A, and N for morning, afternoon and night, respectively) and the second letter denotes whether the office provides complementary electricity for charging (C) or paid charging (P). For example, A-C denotes the scenario for an office worker with working hours starting in the afternoon and the office provides complementary charging.

Fig. 2a shows the total cost in dollars for each approach. As expected, the Opt-V2G approach incurs the lowest cost in all scenarios, significantly reducing expenses compared to Opt-V1G, with more than a 70% reduction (e.g., \$20.3 v.s. \$5.1 in M-C scenario). The Gre-V2G approach also demonstrates substantial cost savings (e.g., \$22.6 v.s. \$7.9 in M-C scenario), highlighting the potential of V2G for reducing expenses. However, compared to Opt-V2G, Gre-V2G still has about a 35% higher cost (e.g., \$7.9 v.s. \$5.1 in M-C scenario).

Fig. 2b depicts CO2 emissions in kilograms. A majority of approaches exhibit ~~zero~~ a low emission since they only charge in the presence of solar energy. @Home has the highest emission (64.9 kg) during the Afternoon shift (A-P, A-C). This is because the majority of the energy charged by the @Home approach occurs directly after working hours. Consequently, the afternoon shift always results in charging brown source energy during peak hours at night. This also contributes to its higher monetary cost in the Afternoon shift (\$39.9). During other working hours, ¬Home has the highest emission (\$36.9) as it constantly charges at a location outside of the home, where energy is sourced from either brown or mixed.

[5] https://www.statista.com/statistics/883118/global-lithium-ion-battery-pack-costs/

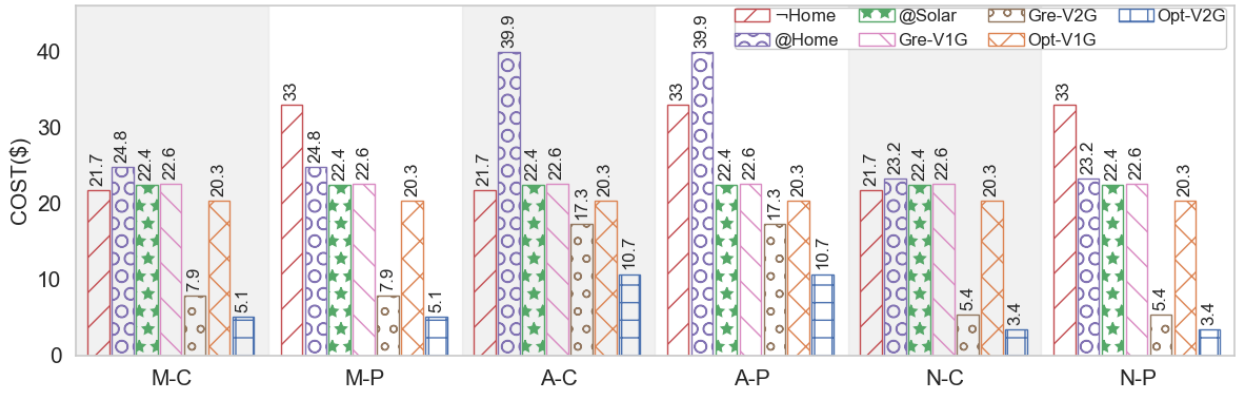

(a) Monetary cost

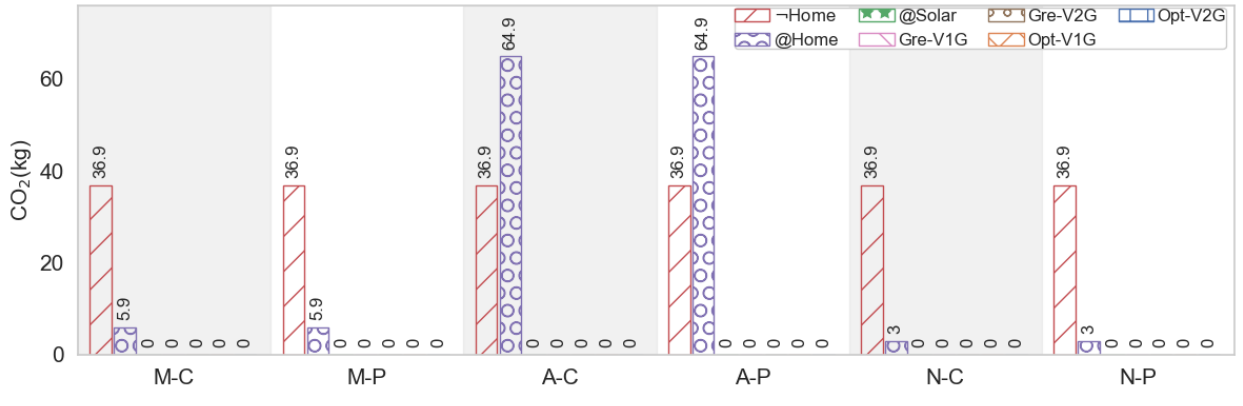

(b) CO2 emissions

Figure 2: Results for different test scenarios for the Office Worker. *M, A* and *N* represent *morning, afternoon* and *night*, respectively, and *C* and *P* represent *complementary* and *paid* electricity at the office, respectively.

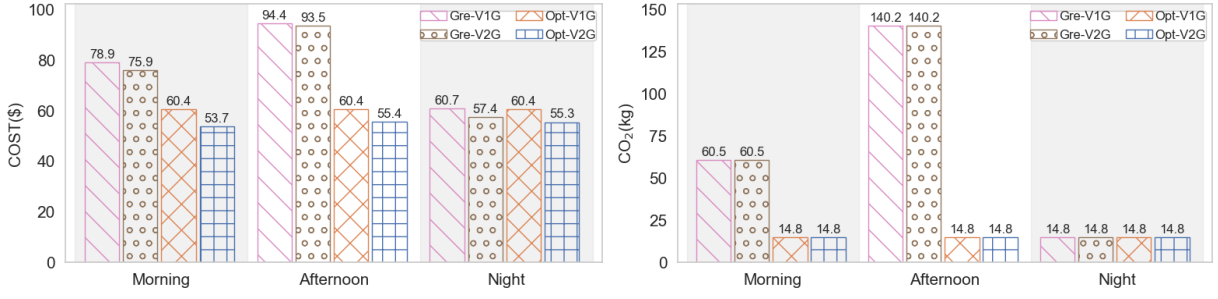

(a) (b)

Figure 3: Results for the Taxi Driver scenarios. @Home, ¬Home and @Solar are omitted because they failed to produce a feasible schedule for these scenarios.

Note that for all work-shifts, there is no difference between the complementary and paid scenarios in terms of both cost and CO_2 emission in both the DP and greedy approaches. The reason is that when $\alpha = 0.5$, charging a mixed-source energy is not preferred, even if it is free. We will explore the impact of α in Sec. 5.4.

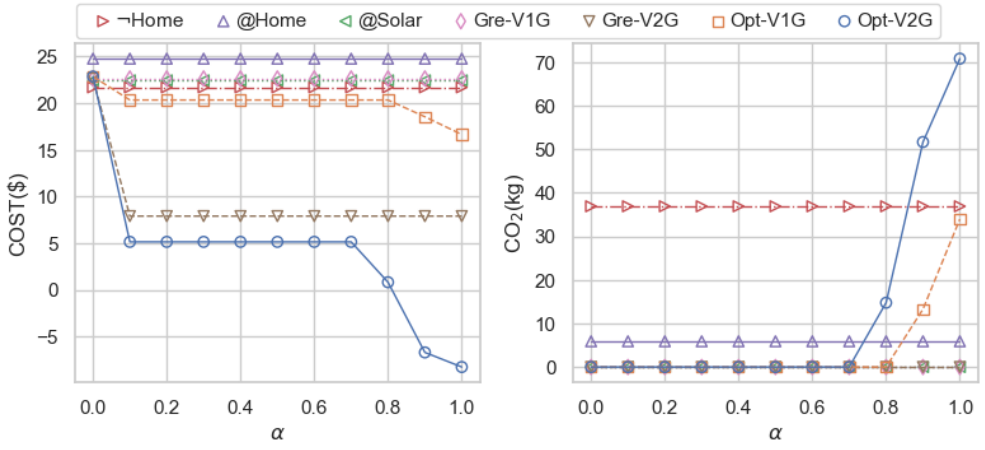

Figure 4: Impact of varying α

5.3.2. Taxi Driver

Fig. 3 shows the impact of various work-shift on our Taxi Driver case study. We exclude *Plug-in approaches* (@Home, ¬Home, @Solar) as they were unable to generate a feasible schedule in these scenarios.

We can see that greedy-based approaches (*Gre-V1G, Gre-V2G*) have a substantial dependency on the work-shift patterns, producing the maximum cost and CO_2 emissions during the afternoon shift (Gre-V1G:\$94.4 and 140.2kg, Gre-V2G:\$93.5 and 140.2kg). Meanwhile, the results from DP-based approaches (*Opt-V1G, Opt-V2G*) appear consistent across all work-shift patterns. The reason is that greedy-based approaches only consider near-future demands when making decisions, resulting in missed opportunities to utilize solar energy in the morning or unnecessary charging with brown energy during peak hours (e.g., charging from 19:00 to 21:00 in the afternoon-shift pattern).

Also, we have noticed that in the Taxi Driver scenarios, *V1G* and *V2G* have similar costs and CO_2 emission. The reason is that there are fewer trading opportunities, as vehicles are typically on the road during working hours.

5.3.3. Summary

In analyzing both cost and CO_2 emissions, Opt-V2G outperforms all baseline approaches. In scenarios typical for office workers, Opt-V2G reduces costs by over 70% compared to V1G approaches and by 35% compared to Gre-V2G, all while maintaining ~~zero~~ a low CO_2 emissions. In scenarios involving taxi drivers, who has limited time slots for decision making and notably longer traveling distance, Opt-V2G consistently achieves the lowest costs and the smallest CO_2 emissions across all work-shift patterns.

5.4. Impact of Variants

5.4.1. Impact of user preference (α)

Fig. 4 presents a comparative analysis of the financial and environmental implications (with an emphasis on CO_2 emissions) resulting from various choices of α. A trend can be observed, where a lower α results in a plan with less CO_2 emissions, while a higher α corresponds to a plan with a reduced cost. Users can choose an α aligning with their preference, for either environmental or financial concerns.

As α increases from 0 to 0.1, there is a significant reduction in the costs associated with Gre-V2G and Opt-V2G. However, the CO_2 emissions remain unchanged. This outcome is due to the selling of surplus solar energy, as evidenced by the fact that both Gre-V2G and Opt-V2G have the same CO_2 emissions as @Solar. Additionally, Opt-V2G achieves a greater cost reduction than Gre-V2G by leveraging information across all time slots to reach the global optimum.

When α increases from 0.1 to 0.7, the plan for each method remains unchanged, as no new trading opportunities arise.

When α exceeds 0.7, Opt-V1G and Opt-V2G begin to significantly reduce their costs while increasing CO_2 emissions. This is due to new trading opportunities that take advantage of complementary charging during office hours (as shown in Table 3). This is evident from the fact that Opt-V1G generates a plan with CO_2 emissions comparable to those of ¬Home.

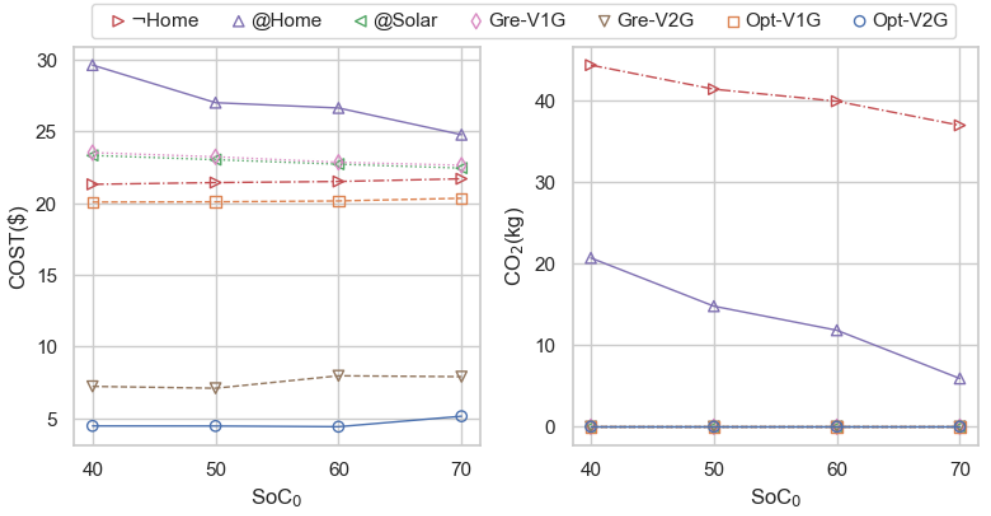

Figure 5: Impact of varying initial SoC levels

5.4.2. Impact of Initial SoC

Fig. 5 displays the results under varying initial SoC levels (SoC_0). It can be seen that the Gre and Opt approaches remain insensitive to SoC_0, whereas @Home and ¬Home approaches have different CO_2. This discrepancy arises because the @Home and ¬Home approaches tend to purchase energy earlier when SoC_0 is smaller to ensure sufficient energy for future use, regardless of energy source and prices fluctuate, as shown in Fig. 3. The @Solar approach generates different plans for the same reason, but their cost and CO_2 emissions are similar, due to the low cost and ~~zero~~ the low CO_2 emission of solar energy.

5.4.3. Impact of Discharging Rate

In practice, the discharging rate often does not match the charging rate. For instance, a charge station may impose restrictions on the discharging rate, or the grid may adjust the discharge rate based on energy demand.

In this series of experiments, we inspect how various discharge rates affect the solution quality. To do this, we apply a scale factor on the discharged energy (Eq (3)) from 0 to 1.2, where 0 means discharging is not allowed, and 1.2 represents the case where the discharge rate is higher than the charge rate. Only V2G approaches are affected in this experiment as other baselines do not make *DIS* decisions.

Fig. 6 illustrates a reduction in costs for V2G approaches as the discharge rate factor increases. This cost reduction is attributed to the greater amount of energy discharged with a higher discharge rate. However, since the discharged energy cannot exceed the charged energy, the curves exhibit unusual fluctuations at higher discharge rate factors.

Moreover, since we preset $\alpha = 0.5$, V2G approaches only trade solar energy, resulting in ~~zero~~ a low CO_2 emission, regardless of the amount of discharged energy.

5.4.4. Impact of Varying Ratio of Selling and Buying Price

In practical settings, the actual profit derived from discharging may not align with our cost model as given in Eq (7). This discrepancy may arise from factors such as fluctuating market prices, driven by supply and demand dynamics, or energy losses during transmission [31], and less energy being sold than was discharged.

To address these scenarios, in this experiment, we study how different levels of profitability affect the solution. Similar to the prior experiment, we apply a scale factor ranging from 0 to 1.2 on Eq (7). Here, a value less than 1 means energy losses during transmission (i.e., smaller $\Delta SoC_i \times B_c$), and a value greater than 1 implies increasing the sell price by the market coordinator (i.e., higher P^{S_i}).

In Fig. 7, we can see a clear trend that the cost of both V2G methods decreases with the scaling factor increases. This pattern is notably stronger when the scaling factor is higher, implying the tendency of both solvers to trade more energy when the factor is higher.

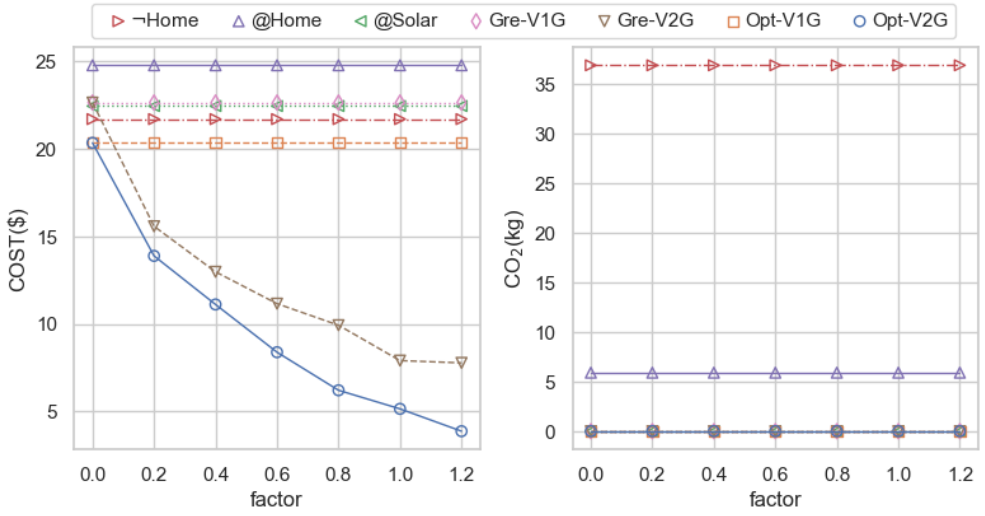

Figure 6: Impact of varying the discharge rate by a factor of the charging rate

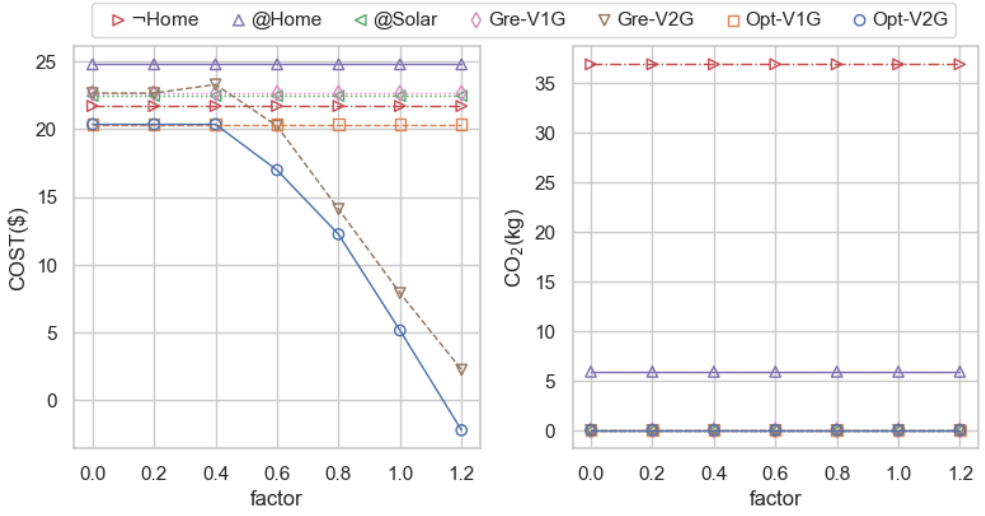

Figure 7: Impact of varying Ratio of Selling and Buying Price

Interestingly, there is a temporary cost rise with the Gre-V2G solver when the factor equals 0.4. The rationale behind this is the fact that, at a factor of 0.4, discharging is unprofitable due to the degradation cost. However, as a greedy-based solver, Gre-V2G cannot anticipate such costs when making charging decisions.

The CO_2 emission from all outlined approaches remains constant, due to the previous discussions in section 5.4.3.

5.4.5. Impact of Travel Energy Usage

In our cost model, for the sake of simplicity, we assume that the driving efficiency (D^E) and the travel distances are constants. However, in practice, these values are affected by various conditions that change over time, such as weather conditions, temperature, or traffic status. Thus, the actual travel energy usage may not align with the Eq (18) ($a = D$). In this experiment, we investigate the impact of varying travel energy usage across different approaches. To perform this analysis, we apply a scaling factor on Eq (18) when *d=DRI*, ranging from 0 to 2.0.

Fig. 8 depicts the results. Note that *solar* is excluded because it does not always find a feasible solution under all scaling factors. From the results, it is clear that increasing travel energy usage increases the cost and CO_2 of both

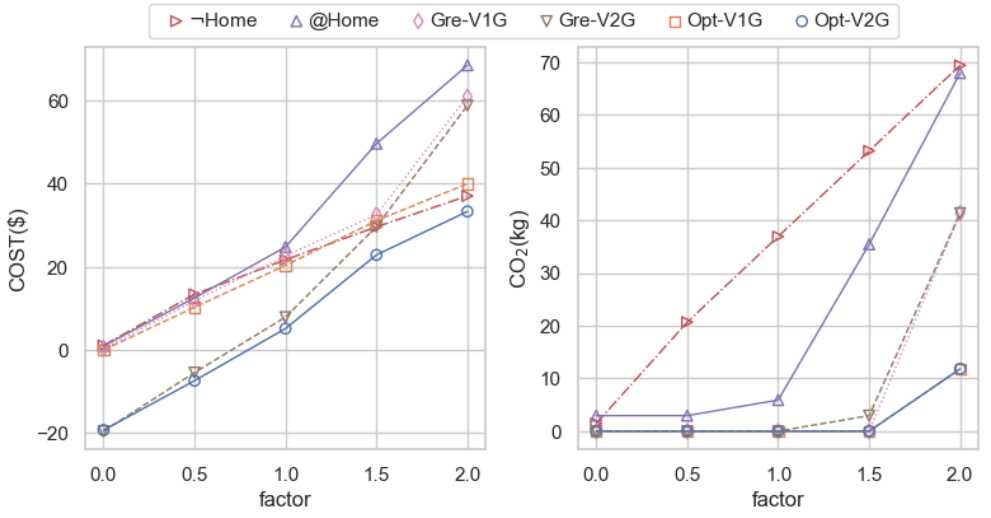

Figure 8: Impact of varying travel energy usage

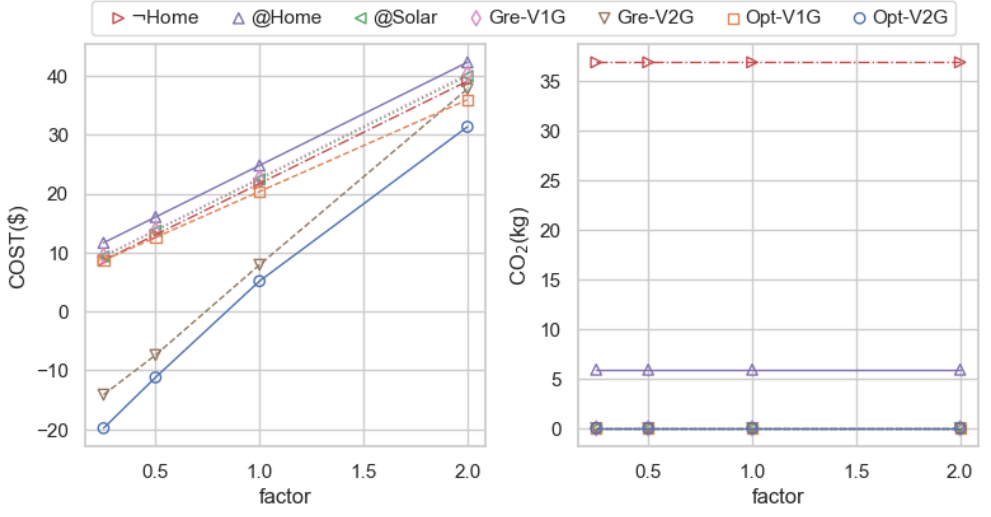

Figure 9: Impact of varying battery degradation cost

methods. As travel energy consumption increases, all methods must accommodate this by charging more energy in their schedules. The Opt-V2G approach only charges solar energy when the factor ≤ 1.5, leading to ~~zero~~ a low CO_2 emission, and the primary costs come from battery degradation. When the factor reaches 2.0, Opt-V2G begins to charge mix-source energy, which is freely available during office hours on weekdays. This leads to in a flattened cost curve and a slight increase in CO_2 emission.

Other approaches behave in similar ways, but their lack of optimal decision making results in significantly higher costs and CO_2 emissions compared to Opt-V2G. For example, ¬Home primarily charges mix-source energy in the office, leading to a nearly linear cost and CO_2 emission curve. @Home, Gre-V1G, and Gre-V2G switch to brown energy source at night time, leading to sharp increases in both cost and CO_2 emissions, particularly at high travel energy usage levels.

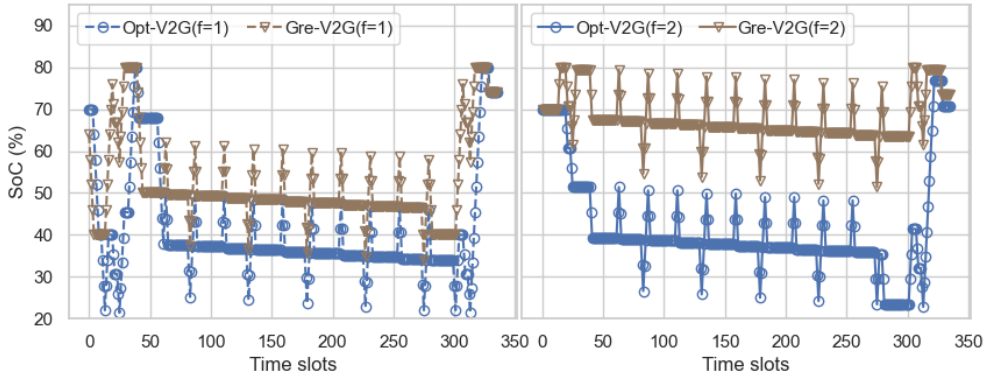

Figure 10: SoC of Opt-V2G and Gre-V2G with different battery degradation factors.

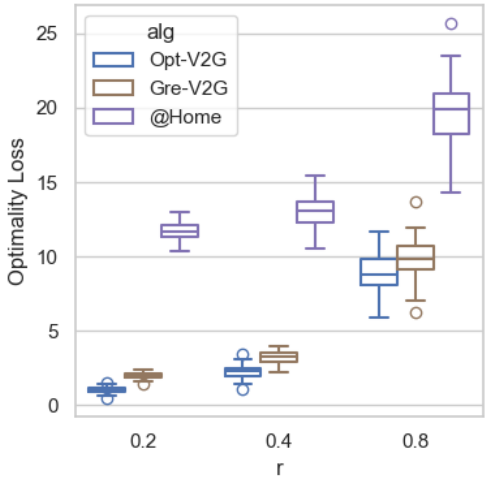

(a)

r	alg	$\Delta Cost$ ($)	ΔCO_2 (kg)	Δobj
0.2	Opt-V2G	2.09	-0.1	1.0
	Gre-V2G	4.51	-0.47	2.02
	@Home	21.47	2.04	11.72
0.4	Opt-V2G	4.47	-0.01	2.27
	Gre-V2G	6.95	-0.34	3.31
	@Home	24.03	2.2	13.05
0.8	Opt-V2G	23.97	-6.46	8.75
	Gre-V2G	26.3	-6.73	9.88
	@Home	44.02	-4.25	19.92

(b)

Figure 11: Optimality Loss with Random Noises. (a) Distribution of Optimality Loss with various ratio (r). (b) The mean of loss on Cost($\Delta Cost$), CO_2(ΔCO_2) and the corresponding optimality loss (Δobj).

5.4.6. Impact of Battery Degradation Cost

The aspect of battery degradation can influence the process of decision-making in V2G. To study this parameter, we applied a scaling factor ranging from 0.25 to 2.0 to Eq (8).

Fig. 9 illustrates that the cost for all approaches changes monotonically with the scaling factor without changing the CO_2 emissions. This indicates that varying the degradation parameter has no impact on the decision-making on the energy source usage.

We also explored how battery degradation cost impacts the overall cost. The cost of degradation, as formulated in Eq (8), is a function of both, the amount of energy discharged and the SoC before discharging. Generally, a higher SoC results in an escalated degradation cost per KWh.

Fig. 10 represents the SoC for all time slots, as obtained by Opt-V2G and Gre-V2G approaches when the scaling factor values are 1 and 2 respectively. We observe that the Opt-V2G approach sustains a comparatively low SoC during weekdays, contributing to a reduced degradation cost. In contrast, the Gre-V2G algorithm shows a higher SoC level when the scaling factor escalates from 1 to 2.

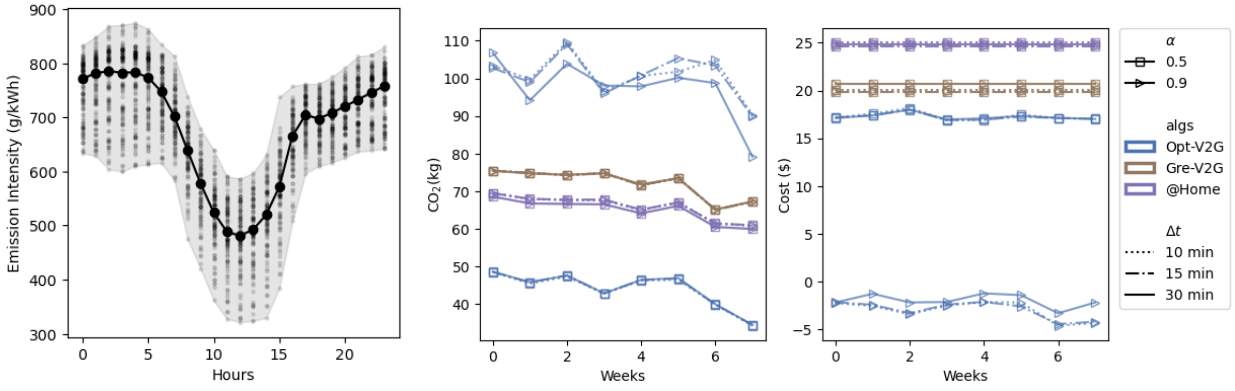

(a) (b)

Figure 12: (a) Distribution of carbon intensity in the dataset group by hour. Median values are described by dots connected by lines, while scatter points illustrate the overall distribution. (b)CO2 and Cost Result

5.4.7. Evaluate Optimality Loss with Random Noises

In practice, some information may consistently change (e.g., energy price) while the schedule being executed, which is referred as random noise. Random noises may cause some less favorable decisions in a schedule be executed, leading to optimality loss. This experiment demonstrates how to use *Opt-V2G* as a yardstick to evaluate optimality loss in the scenario with random noise. To generate random noise, we create 100 instances. For each instance, let a super parameter $r \in (0, 1)$ denote the level of variance, we apply $f_i^B \times P_i^B$ and $f_i^S \times P_i^S$ as the buy and sell price at timeslot i respectively, where f_i^B, f_i^S are randomly sampled from $[1.0 - r, 1.0 + r]$.

To evaluate the optimality loss, we first generate a schedule s using the original prices (i.e., P_i^B, P_i^S), simulating the process of generating the initial schedule. Next, we execute the schedule with random noises (i.e., apply f_i^B, f_i^S on the buy and sell prices) and obtain the objective $obj(s)$, simulating the process of executing a schedule with partial information. We also generate the true optimal schedule that considers random noises, denoted as s^r, intimating the process of back-testing where full-knowledge is available. Then we can evaluate the losses on cost, CO2 and optimality as follows:

$$\begin{cases} \Delta Cost = Cost(s) - Cost(s^r) \\ \Delta CO_2 = CO_2(s) - CO_2(s^r) \\ \Delta obj = obj(s) - obj(s^r), \end{cases}$$

We consider three baselines: the optimal method *Opt-V2G*, the greedy method *Gre-V2G* and a plug-in method @Home. Fig 11(a) shows the distribution of Δobj with $r \in \{0.2, 0.4, 0.8\}$. We can see that the trend of Δobj increases with the variance level r, and *Opt-V2G* has notably smaller Δobj than other baselines. Fig 11(b) shows the mean of $\Delta Cost$, ΔCO_2 and the corresponding Δobj. All entries have $\Delta Cost > 0$ and $\Delta obj > 0$, meaning that they have higher cost and there is some room to further improve the objective. Some entries have $\Delta CO_2 < 0$, indicate that the optimal schedule generates more CO_2 due to actively buying and selling, and the baseline misses such trading opportunity to reduce the cost.

5.5. Results in Real World Dataset

The dataset was obtained from AEMO and includes carbon intensity recorded every 5 minutes for the period from February 6, 2024, to July 27, 2024 (8 weeks). Fig. 12(a) illustrates the distribution of carbon intensities per hour within the dataset. We can see that, in real dataset, 10 to 15 hours of the day tend to have lower carbon intensity, indicating the relative high usage of green energy during this time.

In this experiment, we compare DP (*Opt-V2G*) with a greedy strategy (*Gre-V2G*) and a plug-in approach (@Home). For each method, we fix the planning horizon to one week, and generate 8 schedules for each week independently. For each schedule, we vary $\alpha \in \{0.5, 0.9\}$ and duration per timeslot $\Delta t \in \{10, 15, 30\}$ minutes. To ensure all experiments are conducted at the same ARE level, we scale S along with Δt. Specifically, for $\Delta t \in \{10, 15, 30\}$,

Δt (min)	$\mathcal{S}$	$\lvert\mathbb{T}\rvert$	Runtime(s)	#States
30	10000	336	10.91	1003952.0
15	20000	672	56.39	5668696.0
10	30000	1008	130.75	13232025.0

Table 5
Average runtime and number of states of DP.

we set $\mathcal{S} = 30000, 20000, 10000$ respectively. Note that although $\Delta t = 5$ minutes is available in the dataset, the state space of DP exceeds the memory limit, causing failures when generating a schedule.

Fig. 12(b) presents the sum of cost and CO_2 for each week for various values of α and Δt. For *Opt-V2G*, when $\alpha = 0.5$, the results remain the same across different Δt, suggesting that the EV charges only for daily usage while ignoring all trading opportunities. This is because, in the real dataset, the carbon intensity is high, making the trading decision less favorable. When $\alpha = 0.9$, trading becomes more favorable, and higher granularity offers more trading opportunities. Consequently, $\Delta t = 30$ incurs a relatively higher cost, although the overall difference compared to $\Delta t = 10, 15, 30$ is small. For other baselines, the variance across different values of α and Δt is small, and they consistently generate more CO2 (when $\alpha = 0.5$) or incur more costs (when $\alpha = 0.9$) compared to Opt-V2G.

Table. 5 shows that runtime and number of states of DP increases with $\mathcal{S}$. Note that not all states (i.e., $\lvert\mathbb{T}\rvert \times \mathcal{S}$) are evaluated due to the constraints in DP. We can see that runtime and #States increases faster than the growth of $\mathcal{S}$, and the runtime is strongly correlated with the #States.

6. Conclusion and Future Work

Summary In this work, we proposed a dynamic programming (DP) solver that automatically generates a optimal charging and discharging schedule for EV owners based on prior known informations and their preferences. Our experiments demonstrated several advantages of DP:

- First, in an ideal scenario where carbon-free green energy are periodically available, DP can reduce operational costs by up to 70% by selling surplus energy while achieving ~~zero~~ a low CO_2 emissions.
- Second, by varying the model input parameters, we can observe that the generated schedules are robust, ensuring usability when compared to strategies (Greedy, plug-in) that EV owners commonly use. Specifically, when partially information exists and uncertainty is involved, DP can serve as a yardstick to evaluate optimality loss.
- Third, in real-world scenarios where variance exists in carbon intensity, DP can better aligned with users preferences compared to other baselines.

Limitations Some limitations exist and can be improved in future work:

- **Relying on Full knowledge.** This assumption impacts the feasibility and optimality guarantees of DP when it is applied in real world applications where partially observable information exists, such as energy availability, carbon intensity and energy price. A direction in future work is employing an online-offline framework [21] to reflect real-time information update. Alternatively, predicting the input smartly when generating the schedule might be helpful on the executed result in actual environments [32, 33].
- **No Pareto frontiers.** The limitation of DP is that combining multi-objectives to a single scalar cannot find all Pareto frontiers [34]. In future work, one can employ multi-objective search techniques to efficiently find Pareto frontiers [35], or develop an interactive framework for users so that the schedule aligns precisely with their preferences.
- **Only for single EV.** The state space of DP only considers a single EV. However, in some scenarios, decision among multiple EVs may be coupled. For example, a family with multiple EVs may have only one charging point at home. An interesting direction in future work is extending the scenario when multiple EVs are involved.

Acknowledgement

Muhammad Aamir Cheema and Adel N. Toosi are supported by Australian Research Council DP230100081

References

[1] Paris declaration on electro-mobility and climate change & call to action (2015).
URL https://unfccc.int/media/521376/paris-electro-mobility-declaration.pdft

[2] Electric vehicle market size, trends, growth, report 2022-2030 (2022).
URL https://www.precedenceresearch.com/electric-vehicle-market

[3] B. K. Sovacool, R. F. Hirsh, Beyond batteries: An examination of the benefits and barriers to plug-in hybrid electric vehicles (phevs) and a vehicle-to-grid (v2g) transition, Energy Policy 37 (3) (2009) 1095–1103. doi:https://doi.org/10.1016/j.enpol.2008.10.005.
URL https://www.sciencedirect.com/science/article/pii/S0301421508005934

[4] Australian Bureau of Statistics, Survey of motor vehicle use, australia, Accessed 2024 April 3 (June 2020).
URL https://www.abs.gov.au/statistics/industry/tourism-and-transport/survey-motor-vehicle-use-australia/latest-release

[5] M. A. Cheema, H. Wang, W. Wang, A. N. Toosi, E. Tanin, J. Qi, H. Samet, Beyond the commute: Unlocking the potential of electric vehicles as future energy storage solutions (vision paper), in: Proceedings of the 32nd ACM International Conference on Advances in Geographic Information Systems, SIGSPATIAL 2024, Atlanta, GA, USA, 29 October 2024 - 1 November 2024, 2024, pp. 469–472. doi:10.1145/3678717.3691247.

[6] B. Shen, J. Du, M. A. Cheema, Beyond transport: V2X integration turning EVs into smart energy assets, in: Proceedings of the 33rd ACM International Conference on Advances in Geographic Information Systems SIGSPATIAL 2025, Minneapolis, MN, USA, 3 November 2025 - 6 November 2025, 2025.

[7] A. Blatiak, F. Bellizio, L. Badesa, G. Strbac, Value of optimal trip and charging scheduling of commercial electric vehicle fleets with vehicle-to-grid in future low inertia systems, CoRR abs/2204.11565 (2022).

[8] P. Liu, C. Wang, J. Hu, T. Fu, N. Cheng, N. Zhang, X. Shen, Joint route selection and charging discharging scheduling of evs in V2G energy network, IEEE Trans. Veh. Technol. 69 (10) (2020) 10630–10641. doi:10.1109/TVT.2020.3018114.
URL https://doi.org/10.1109/TVT.2020.3018114

[9] Z. Cao, C. P. Chu, R. Gadh, An autonomous electric vehicle based charging system: Matching and charging strategy, in: ISGT, IEEE, 2018, pp. 1–5.

[10] X. Lee, H. Yang, W. Tang, A. N. Toosi, E. Lam, An adaptive charging scheduling for electric vehicles using multiagent reinforcement learning, in: Service-Oriented Computing - 19th International Conference, ICSOC 2021, Virtual Event, November 22-25, 2021, Proceedings, Vol. 13121 of Lecture Notes in Computer Science, Springer, 2021, pp. 273–286. doi:10.1007/978-3-030-91431-8_17.

[11] Y. Cao, H. Song, O. Kaiwartya, B. Zhou, Y. Zhuang, Y. Cao, X. Zhang, Mobile edge computing for big-data-enabled electric vehicle charging, IEEE Communications Magazine 56 (3) (2018) 150–156.

[12] J. Du, B. Shen, M. A. Cheema, A. N. Toosi, Smart ride and delivery services with electric vehicles: Leveraging bidirectional charging for profit optimisation, Information Sciences 732 (2026) 122929. doi:https://doi.org/10.1016/j.ins.2025.122929.
URL https://www.sciencedirect.com/science/article/pii/S0020025525010655

[13] D. Pelosi, M. Longo, D. Zaninelli, L. Barelli, Experimental investigation of fast- charging effect on aging of electric vehicle li- ion batteries, Energies 16 (18) (2023) 6673.

[14] S. Li, P. Zhao, C. Gu, J. Li, D. Huo, S. Cheng, Aging mitigation for battery energy storage system in electric vehicles, IEEE Transactions on Smart Grid 14 (3) (2022) 2152–2163.

[15] N. Daina, A. Sivakumar, J. W. Polak, Electric vehicle charging choices: Modelling and implications for smart charging services, Transportation Research Part C: Emerging Technologies 81 (2017) 36–56.

[16] H. Krueger, A. Cruden, Integration of electric vehicle user charging preferences into vehicle-to-grid aggregator controls, Energy reports 6 (2020) 86–95.

[17] M. Alinejad, O. Rezaei, A. Kazemi, S. Bagheri, An optimal management for charging and discharging of electric vehicles in an intelligent parking lot considering vehicle owner's random behaviors, Journal of Energy Storage 35 (2021) 102245.

[18] Z. Zhao, C. K. Lee, J. Ren, A two-level charging scheduling method for public electric vehicle charging stations considering heterogeneous demand and nonlinear charging profile, Applied Energy 355 (2024) 122278. doi:https://doi.org/10.1016/j.apenergy.2023.122278.
URL https://www.sciencedirect.com/science/article/pii/S0306261923016422

[19] B. Aljafari, P. R. Jeyaraj, A. C. Kathiresan, S. B. Thanikanti, Electric vehicle optimum charging-discharging scheduling with dynamic pricing employing multi agent deep neural network, Computers and Electrical Engineering 105 (2023) 108555. doi:https://doi.org/10.1016/j.compeleceng.2022.108555.
URL https://www.sciencedirect.com/science/article/pii/S0045790622007704

[20] A. Saldarini, M. Longo, W. Yaici, Smart charging strategies for evs: Insights from simulation modeling on italian highways, IEEE Access (2025) 1–1doi:10.1109/ACCESS.2025.3538094.

[21] A. Koufakis, E. S. Rigas, N. Bassiliades, S. D. Ramchurn, Offline and online electric vehicle charging scheduling with V2V energy transfer, IEEE Trans. Intell. Transp. Syst. 21 (5) (2020) 2128–2138.

[22] W. Yang, J. Guo, A. Vartosh, Optimal economic-emission planning of multi-energy systems integrated electric vehicles with modified group search optimization, Applied Energy 311 (2022) 118634.

[23] R. Li, S. SaeidNahaei, Optimal operation of energy hubs integrated with electric vehicles, load management, combined heat and power unit and renewable energy sources, Journal of Energy Storage 48 (2022) 103822.

[24] J. Dixon, W. Bukhsh, C. Edmunds, K. Bell, Scheduling electric vehicle charging to minimise carbon emissions and wind curtailment, Renewable Energy 161 (2020) 1072–1091.

[25] B. Shimaa, I. O. Ahmed, T.-E. Elsayed, A. T. Ahmad, M. A. Hala, S. M.M., Achieving green mobility: Multi-objective optimization for sustainable electric vehicle charging, Energy Strategy Reviews 53 (2024) 101351. doi:https://doi.org/10.1016/j.esr.2024.101351.
URL https://www.sciencedirect.com/science/article/pii/S2211467X24000580

[26] M. Xu, T. Wu, Z. Tan, Electric vehicle fleet size for carsharing services considering on-demand charging strategy and battery degradation, Transportation Research Part C: Emerging Technologies 127 (2021) 103146.

[27] Victoria default offer, https://www.esc.vic.gov.au/electricity-and-gas/prices-tariffs-and-benchmarks/victorian-default-offer, accessed: 26-July-2023 (2023).

[28] B. Metz, O. Davidson, H. De Coninck, M. Loos, L. Meyer, Ipcc special report on carbon dioxide capture and storage, Cambridge: Cambridge University Press, 2005, Ch. 10, p. 347.

[29] Electric vehicle database, byd-atto-3, accessed 2024 April 3 (2024).
URL https://ev-database.org/car/1782/BYD-ATTO-3

[30] Charger types and speeds, accessed 2024 April 3 (2024).
URL https://www.transportation.gov/rural/ev/toolkit/ev-basics/charging-speeds

[31] Y. A. Shirazi, D. L. Sachs, Comments on "measurement of power loss during electric vehicle charging and discharging"–notable findings for v2g economics, Energy 142 (2018) 1139–1141.

[32] M. I. Al-Amin, J. Du, M. A. Cheema, I. F. Siddiqui, M. Salehi, EV energy trading dashboard: Cost-emission reduction through spatiotemporal forecasts and smart charging, in: Proceedings of the 33rd ACM International Conference on Advances in Geographic Information Systems SIGSPATIAL 2025, Minneapolis, MN, USA, 3 November 2025 - 6 November 2025, 2025.

[33] A. N. Elmachtoub, P. Grigas, Smart "predict, then optimize", Management Science 68 (1) (2022) 9–26.

[34] N. Rivera, J. A. Baier, C. Hernández, Subset approximation of pareto regions with bi-objective A, in: Thirty-Sixth AAAI Conference on Artificial Intelligence, AAAI 2022, Thirty-Fourth Conference on Innovative Applications of Artificial Intelligence, IAAI 2022, The Twelveth Symposium on Educational Advances in Artificial Intelligence, EAAI 2022 Virtual Event, February 22 - March 1, 2022, AAAI Press, 2022, pp. 10345–10352. doi:10.1609/aaai.v36i9.21276.
URL https://doi.org/10.1609/aaai.v36i9.21276

[35] L. Mandow, J.-L. Pérez de la Cruz, Improving bi-objective shortest path search with early pruning, ECAI 2023 (2023) 1680–1687.